ISSN 1674-1056
http://cpb.iphy.ac.cn
http://iopscience.iop.org/cpb
中国物理 B
Chinese Physics
中国物理 Chinese Physics B

Two-dimensional electron gas characteristics of InP-based high electron mobility transistor terahertz detector

Jin-Lun Li(李金伦), Shao-Hui Cui(崔少辉), Jian-Xing Xu(徐建星), Xiao-Ran Cui(崔晓然), Chun-Yan Guo(郭春妍), Ben Ma(马奔), Hai-Qiao Ni(倪海桥), Zhi-Chuan Niu(牛智川)
Citation: Chin. Phys. B . 2018, 27(4): 047101. **doi:** 10.1088/1674-1056/27/4/047101

Journal homepage: http://cpb.iphy.ac.cn; http://iopscience.iop.org/cpb

What follows is a list of articles you may be interested in

Low specific on-resistance GaN-based vertical heterostructure field effect transistors with nonuniform doping superjunctions

Wei Mao(毛维), Hai-Yong Wang(王海永), Peng-Hao Shi(石朋毫), Xiao-Fei Wang(王晓飞), Ming Du(杜鸣), Xue-Feng Zheng(郑雪峰), Chong Wang(王冲), Xiao-Hua Ma(马晓华), Jin-Cheng Zhang(张进成), Yue Hao(郝跃)
Chin. Phys. B . 2018, 27(4): 047305. **doi:** 10.1088/1674-1056/27/4/047305

Simulation study of InAlN/GaN high-electron mobility transistor with AlInN back barrier

Tie-Cheng Han(韩铁成), Hong-Dong Zhao(赵红东), Lei Yang(杨磊), Yang Wang(王杨)
Chin. Phys. B . 2017, 26(10): 107301. **doi:** 10.1088/1674-1056/26/10/107301

Electrical property effect of oxygen vacancies in the heterojunction of $LaGaO_3/SrTiO_3$

Fu-Ning Wang(王芙凝), Ji-Chao Li(李吉超), Xin-Miao Zhang(张鑫淼), Han-Zhang Liu(刘汉璋), Jian Liu(刘剑), Chun-Lei Wang(王春雷), Ming-Lei Zhao(赵明磊), Wen-Bin Su(苏文斌), Liang-Mo Mei(梅良模)
Chin. Phys. B . 2017, 26(3): 037101. **doi:** 10.1088/1674-1056/26/3/037101

Low-resistance Ohmic contact on polarization-dopedAlGaN/GaN heterojunction

Li Shi-Bin, Yu Hong-Ping, Zhang Ting, Chen Zhi, Wu Zhi-Ming
Chin. Phys. B . 2014, 23(10): 107101. **doi:** 10.1088/1674-1056/23/10/107101

Some corrections to the Thomas–Fermi theory

Janusz Chrzanowski
Chin. Phys. B . 2013, 22(8): 087101. **doi:** 10.1088/1674-1056/22/8/087101

Two-dimensional electron gas characteristics of InP-based high electron mobility transistor terahertz detector*

Jin-Lun Li(李金伦)[1,2], Shao-Hui Cui(崔少辉)[1], Jian-Xing Xu(徐建星)[2,4], Xiao-Ran Cui(崔晓然)[2,5], Chun-Yan Guo(郭春妍)[2,6], Ben Ma(马奔)[2,3], Hai-Qiao Ni(倪海桥)[2,3,†], and Zhi-Chuan Niu(牛智川)[2,3]

[1] *Department of Missile Engineering, Shijiazhuang Campus, Army Engineering University, Shijiazhuang* 050003, *China*
[2] *State Key Laboratory for Superlattices, Institute of Semiconductors, Chinese Academy of Sciences (CAS), Beijing* 100083, *China*
[3] *College of Materials Science and Opto-Electronic Technology, University of Chinese Academy of Sciences, Beijing* 100049, *China*
[4] *Microsystem & Terahertz Research Center, China Academy of Engineering Physics, Chengdu* 610200, *China*
[5] *Wide Bandgap Semiconductor Technology Disciplines State Key Laboratory, Xidian University, Xi'an* 710071, *China*
[6] *Key Laboratory of Ultra-fast Photoelectric Diagnostics Technology of Chinese Academy of Sciences, Xi'an Institute of Optics and Precision Mechanics, Xi'an* 710119, *China*

(Received 1 December 2017; revised manuscript received 24 December 2017; published online 10 March 2018)

The samples of $In_xGa_{1-x}As/In_{0.52}Al_{0.48}As$ two-dimensional electron gas (2DEG) are grown by molecular beam epitaxy (MBE). In the sample preparation process, the In content and spacer layer thickness are changed and two kinds of methods, i.e., contrast body doping and δ-doping are used. The samples are analyzed by the Hall measurements at 300 K and 77 K. The $In_xGa_{1-x}As/In_{0.52}Al_{0.48}As$ 2DEG channel structures with mobilities as high as 10289 $cm^2/V{\cdot}s$ (300 K) and 42040 $cm^2/V{\cdot}s$ (77 K) are obtained, and the values of carrier concentration (N_c) are $3.465\times10^{12}/cm^2$ and $2.502\times10^{12}/cm^2$, respectively. The THz response rates of InP-based high electron mobility transistor (HEMT) structures with different gate lengths at 300 K and 77 K temperatures are calculated based on the shallow water wave instability theory. The results provide a reference for the research and preparation of InP-based HEMT THz detectors.

Keywords: THz detector, high electron mobility transistor, two-dimensional electron gas, InP

PACS: 71.10.Ca, 73.40.Kp, 81.05.Ea **DOI:** 10.1088/1674-1056/27/4/047101

1. Introduction

A terahertz (THz) wave refers to the wave with a frequency between 0.1 THz–10 THz, and its corresponding wavelength is in a range of 3 mm–30 μm, so it is located between the infrared and millimeter waves. The terahertz wave is in the transition region from electronics to photonics. It overlaps with the infrared ray in the short band and crosses the long wave band with the millimeter wave. It occupies a very special position in the electromagnetic radiation spectrum.[1] Because of its band specificity, terahertz waves exhibit many unique physical properties, such as i) broad spectral properties: thousands of GHz bands, bandwidth growth is obvious for 5G communication currently being developed (20 GHz–40 GHz); ii) transient: the typical pulse time of pulse terahertz radiation is generally below picosecond, which can be used for ultrafast time resolution study of materials; iii) strong penetration: terahertz radiation can penetrate most non-polar materials, such as wood, textiles and plastic products, and it can be widely used in special fields such as security inspection, anti-terrorism, etc.; iv) low energy: compared with the single photon energy of an x-ray, 1-THz single photon energy is only 4.1 meV, less than 1% of the x-ray, and the THz radiation has no effect on the ionization of substances in a medical examination, and it can play an important role in human security because it cannot be involved in the x-ray.[2] After nearly 40 years of development, with the progress of material technology and micro-nano processing technology, the terahertz band electronics and photonics technology is developing rapidly.[3]

The development of terahertz technology cannot be separated from the research of terahertz detectors. At present, the research of terahertz detection mainly focuses on the Schottky diode, thermal detector, superconducting SIS detector, photoconductive antenna, etc.[4] Among these techniques, the Schottky diode is limited to its lower frequency response ($<$ 1 THz), thermal radiometer detection due to the slow response speed, the low temperature superconducting SIS detector in use, the photoconductive antenna sensitivity is low, and it needs to cooperate with the transmit antenna. In 1993, Dyakonov *et al.* proposed a theory that in high electron mobility materials, there is a "shallow wave" whose frequency is in the terahertz range and it can respond to terahertz radiation.[5] Such a theory has been constantly validated in the following 20 years.[6–9] The fabricated device is known as the HEMT field effect terahertz detector.

Dyakonov *et al.* proposed that in boundary conditions, 2DEG in the HEMT structure, if the channel length L is much

*Project supported by the Foundation for Scientific Instrument and Equipment Development, Chinese Academy of Sciences (Grant No. YJKYYQ20170032) and the National Natural Science Foundation of China (Grant No. 61435012).

†Corresponding author. E-mail: nihq@semi.ac.cn

© 2018 Chinese Physical Society and IOP Publishing Ltd

less than the mean free path of a particle, but larger than the average distance between electron and electron collision, it can be analogous to the Euler equation in fluid mechanics.[10] Even when the electron velocity v_0 is less than the plasma wave velocity, the 2DEG will become unstable, and then the electromagnetic wave will be generated by the oscillation. The electromagnetic frequency can be modulated by the gate voltage and can be modulated to reach the terahertz band. The first experiment to observe the phenomenon of HEMT response to terahertz radiation was conducted in 1998.[11]

At present, however, the frequency of the near-terahertz detector is generally below 100 GHz, and the azimuthal resolution of the imaging is generally less than 5 mm. In order to improve the recognition of contraband, the resolution still needs to be further improved. The use of high frequency terahertz wave is the most fundamental way to improve the resolution of imaging. By using the terahertz wave with an incident frequency of 200 GHz, the resolution is expected to increase to submillimeter.

2. Experiment

The HEMT epitaxial structures of the terahertz detector were grown on InP (100) substrates with Fe-doped by a VEECO Gen-930 system, which is made in the United States. The surface deoxidation process of InP is monitored synchronously by reflection high energy electron diffraction (RHEED).[12] Until a reconstruction (2×4) was observed, the reconstruction temperature (T_c) was recorded. The reconstructed images by RHEED are shown in Fig. 1. Before the growing of HEMT structure, the substrate should be heated to 615 °C ($T_c + 40$ °C) for 4 min with a heating rate of 20 °C ramp under As_2 overpressure.

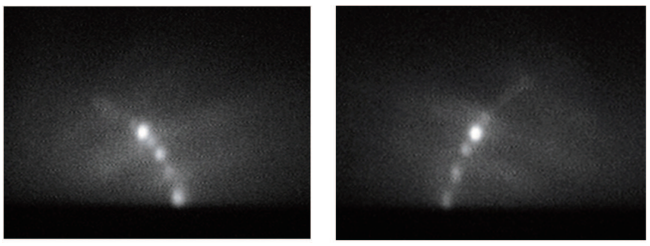


Fig. 1. Reconstructed images by RHEED.

The basic HEMT THz detector is a 2DEG structure, so in order to analyze the influences of material parameter on carrier concentration and mobility, the In content (x_{In}), spacer and channel layer thickness, body doping and δ-doping were compared. The basic sample structure is shown in Table 1. The 2DEG structure is (from bottom to top): 400-nm-thick $In_{0.52}Al_{0.48}As$ buffer layer over the InP semi insulating substrate, 10-nm-thick $In_xGa_{1-x}As$ channel layer, W_d-thick $In_{0.52}Al_{0.48}As$ spacer layer, Si δ-doping layer with doping 5×10^{12} cm^{-2}, 14-nm-thick $In_{0.52}Al_{0.48}As$ barrier, 10-nm-thick $In_{0.53}Ga_{0.47}As$ cap layer with 3×10^{18} cm^{-3} doping, and finally 10-nm-thick $In_{0.65}Ga_{0.35}As$ cap layer with 5×10^{18} cm^{-3} doping.

Table 1. Basic sample structure of $In_xGa_{1-x}As/In_{0.52}Al_{0.48}As$ HEMT.

Layer	Thickness/nm	Doping/cm^{-3}
$In_{0.65}Ga_{0.35}As$ cap1	10	5×10^{18}
$In_{0.53}Ga_{0.47}As$ cap2	10	3×10^{18}
$In_{0.52}Al_{0.48}As$ barrier	14	undoped
Si δ-doping		5×10^{12} cm^{-2}
$In_{0.52}Al_{0.48}As$ spacer	W_d	undoped
$In_xGa_{1-x}As$ channel	10	undoped
$In_{0.52}Al_{0.48}As$ buffer	400	undoped
InP semi insulating substrate		

The InP-based structure was grown on an Fe-doped substrate at T_c–10 °C temperature, and a growth interruption under As_2 overpressure was used at the InGaAs/$In_{0.52}Al_{0.48}As$ interfaces.[13] The lowest surface roughness was observed. As shown in Fig. 2, the atomic step can be observed obviously by AFM measurement with a scanning range of 10 μm×10 μm.

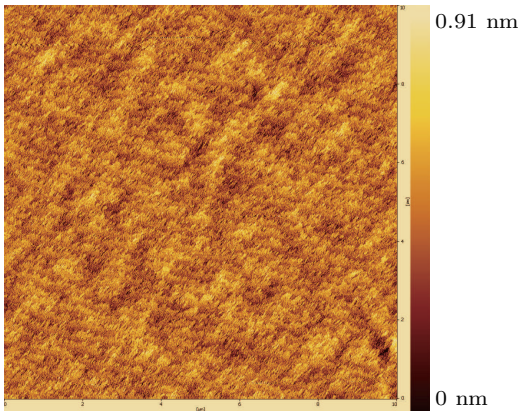


Fig. 2. (color online) AFM image of sample surface under T_c-10 °C growth temperature.

The prepared samples were characterized by Hall measurement of the four-probe Van der Pauw measurement structure. The sample size was 1 cm×1 cm square. Before the measurement, the metal indium was positioned around the sample to ohmically contact the electrode. In the measurement process, the magnetic field was 0.5 T, and the current was 100 μA. The carrier mobilities and carrier concentrations of the samples were measured at room temperature and 77 K.

3. Results and analysis

3.1. Channel layer In content

In order to verify the influences of different In content conditions on the characteristics of $In_xGa_{1-x}As/In_{0.52}Al_{0.48}As$ 2DEG, a set of different samples are obtained by changing the In fraction in the sample preparation process, in which the In fractions are 0.65, 0.70, 0.75, and 0.80, respectively. In

order to ensure that the measurement results are comparable with each other, the thickness of the spacer layer is defined as 3 nm, and the δ-doping method is adopted. The Hall measurement results are shown in Fig. 3. A maximum carrier mobility of $\mu = 10289$ cm^2/V·s with a carrier concentration of $N_c = 3.465 \times 10^{12}$/cm^2 at 300 K is obtained with the channel In content of 0.75. The Hall measurement at 77 K displays a carrier mobility as high as $\mu = 42040$ cm^2/V·s with a carrier concentration of $N_c = 2.502 \times 10^{12}$/cm^2.

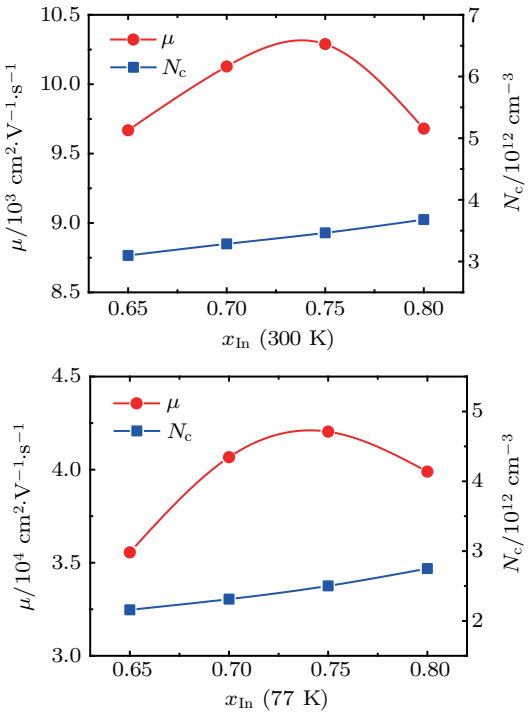


Fig. 3. (color online) Carrier mobilities and carrier concentrations with different In content at 300 K and 77 K.

From the measurement results in Fig. 3, the carrier mobility (μ) and carrier concentration (N_c) increase with In content increasing. The reason for the increase of carrier concentration (N_c) is analyzed. This is due to the lower conduction band energy (E_c) of InAs, it is considered that there is a direct relationship between the In content and the barrier height in the $In_xGa_{1-x}As/In_{0.52}Al_{0.48}As$ interface, and there is a linearly increasing relationship between them. A high In content will also weaken the alloy disorder scattering of 2DEG.[13]

The change of mobility is due to the smaller barrier height and stronger ionization impurity scattering at $x_{In} = 0.65$, leading to lower mobility. When the In content increases, the ionization impurity scattering becomes weaker and the mobility increases. Of course, the high value of In content will be detrimental to the heterojunction matching, and the band gap will change from direct transition to indirect transition, which is unfavorable for the mobility.

3.2. Spacer layer thickness

In order to verify the effect of different spacer layer thicknesses on the two-dimensional electron gas characteristics of $In_xGa_{1-x}As/In_{0.52}Al_{0.48}As$, the experimental group is set to be of the δ-doping mode, the thickness values of the spacer layer are set to be 2 nm, 3 nm, 4 nm, 5 nm, and 6 nm, and the Hall measurement results are shown in Fig. 4.

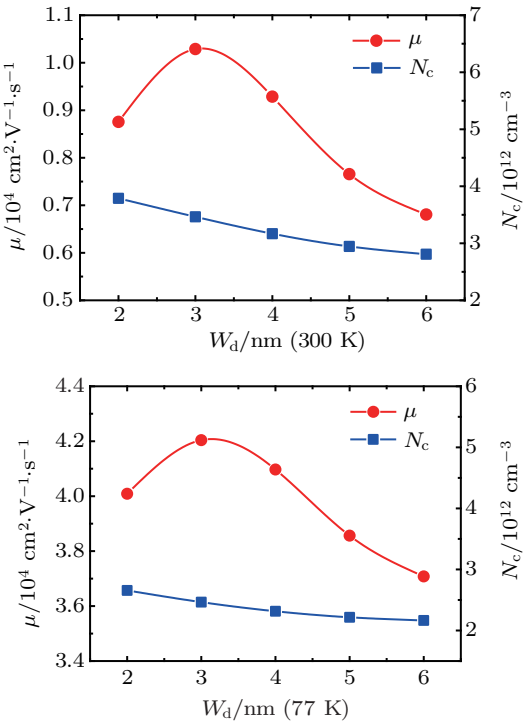


Fig. 4. (color online) Results of Hall measurement with different spacer layer thickness.

From the measurement results of Fig. 4, it can be seen that the carrier concentration of $In_xGa_{1-x}As/In_{0.52}Al_{0.48}As$ 2DEG decreases and the mobility decreases with the thickness of the spacer layer increasing. According to the triangular potential well model[13] proposed by Stern, the expression of the carrier concentration of 2DEG can be obtained by solving the Schrodinger equation and Poisson equation of 2DEG[14] as follows:

$$N_c = \sqrt{2\varepsilon_1 N_d V_{20}/q + N_d^2 W_d^2} - N_d W_d.$$

In the formula, ε_1 is the relative dielectric constant of InAlAs material; V_{20} is the potential energy difference at the two ends of the spacer layer; N_d is the δ-doping concentration; W_d represents the spacer layer thickness. It can be seen from the formula that when the δ-doping concentration (N_d) and In content are fixed, the carrier concentration (N_c) decreases with the spacer layer thickness (W_d) increasing, which is consistent with the experimental results.

The mobility first increases and then decreases, and the analyses show that when the spacer layer is thin, the remote ionized impurity scattering is weak, which leads to the mobility increasing; and when the spacer layer increases while the carrier concentration decreases, the shielding effect of 2DEG on the remote ionized impurity scattering weakens, so in the two kinds of factors, the mobility reaches a peak between 3 nm and 4 nm. Therefore, it is reasonable to choose the thickness of the spacer layer to be between 3 nm and 4 nm by combining

the measurement results and the limit of shutter speed of the MBE system.

3.3. Doping method and condition

In order to compare the effects of bulk doping and δ-doping on the 2DEG characteristics, the $In_{0.52}Al_{0.48}As$ barrier layer with 14-nm thickness is doped, due to the doping concentration of δ-doping being 5×10^{12} cm^{-2}. According to the growth thickness and growth time, the bulk doping concentration is converted to 3.57×10^{18} cm^{-3}. Other growth conditions and sample structure are consistent with those discussed above.

Hall measurement is used to measure the mobilities and carrier concentrations of the samples. The measurement results are shown in Table 2. Under the same conditions, the mobility of the sample with δ-doping is 10289 cm^2/V·s, and the carrier concentration is 3.465×10^{12}/cm^2 at 300 K, which is much higher than those of the bulk doping samples. Therefore, the δ-doping is a kind of high doping concentration, which can effectively improve the carrier density in the channel.[15]

Table 2. Hall measurement results of two different doping modes.

Doping method	Mobility /(cm^2/V·s)	Carrier concentration /cm^{-2}	Hall coefficient /(cm^3/C)
$\delta-$doping	10289	3.465×10^{12}	-1.804×10^{6}
	10279	3.462×10^{12}	-1.805×10^{6}
Bulk-doping	9329	2.039×10^{12}	-1.065×10^{6}
	9318	2.027×10^{12}	-1.066×10^{6}

4. Effect of gate length on terahertz response rate

One of the parameters that affect the response rate of HEMT structure to THz is the gate length. By changing the gate length, the oscillation response of the device can be adjusted.[16,17] But for the device structure shown in Fig. 5, the gate length is fixed, and the response rates of different gate lengths to the terahertz wave cycle are longer and the cost is higher in an experiment. Therefore, the Wolfram Mathematica 11.0 software is used before the specific process, according to the actual situation of molecular beam epitaxy and the shallow water waves instability theory proposed by Dyakonov.[10]

It is proposed that the detector response be the constant source-to-drain voltage induced by the incoming terahertz signal

$$\frac{\Delta U}{U_0}=\frac{1}{4}\left(\frac{U_{\rm ac}}{U_0}\right)^2 f(\omega),$$

where

$$f(\omega)=1+\beta-\frac{1+\beta\cos(2k_0'L)}{\sinh^2(k_0''L)+\cos^2(k_0'L)}.$$

Here

$$\beta=\frac{2\omega\tau}{\sqrt{1+(\omega\tau)^2}},$$

ω is the angular frequency of the incident terahertz wave, τ is the electron collision time with phonons and impurities, and k_0 is the dispersion relation for the plasma waves, k_0' and k_0'' are the real and imaginary part of k_0, and given as follows:

$$k_0'=\frac{\omega}{s}\left(\frac{\left(1+w^{-2}\tau^{-2}\right)^{1/2}+1}{2}\right)^{1/2},$$

$$k_0''=\frac{\omega}{s}\left(\frac{\left(1+w^{-2}\tau^{-2}\right)^{1/2}-1}{2}\right)^{1/2}.$$

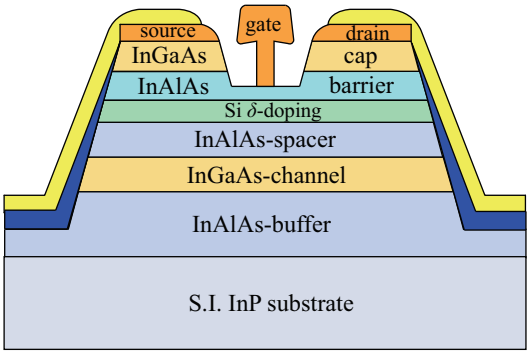


Fig. 5. (color online) Schematic diagram of device structure.

The detector responsivity is defined as[18]

$$R=R_0 f(\omega),$$

where

$$R_0=\frac{\pi}{8GcU_0}.$$

Here, c is the speed of light, $U_0=U_{\rm gs}-U_{\rm T}$, with $U_{\rm T}$ being the threshold voltage, and $U_{\rm gs}$ the gate-to-source voltage. Symbol s denotes the velocity of the plasma wave. Gain of coupled antenna $G=8$, which is the typical value of a bowtie antenna.[19]

The terahertz response rates of the gate lengths of 0.5 μm, 2 μm, and 5 μm are calculated at 300 K and 77 K, respectively. The simulation parameters of the material samples are obtained experimentally and the relavent InGaAs channel material parameters are shown in Table 3.

Table 3. Related parameters of theoretical calculation.

Temperature /K	Effective mass $/(m/m_0)$	Mobility /(cm^2/V·s)	Carrier concentration /cm^{-2}	Viscosity /(cm^2/s)
77	0.041	42040	2.502×10^{12}	26
300		10289	3.465×10^{12}	780

Due to the fact that the 2DEG plasmon wave vector is mismatched with the free space terahertz optical wave vector, the interaction between the plasmons and the free space terahertz wave needs to be realized through a suitable coupling structure.[3] The commonly used coupling structures are grating,[20] bow tie antenna,[21] logarithmic periodic antenna,[22] etc. A bow tie antenna coupling structure is used in this paper.

Taking the parameters into a simulation, the theoretical response rate can be obtained as shown in Fig. 6.

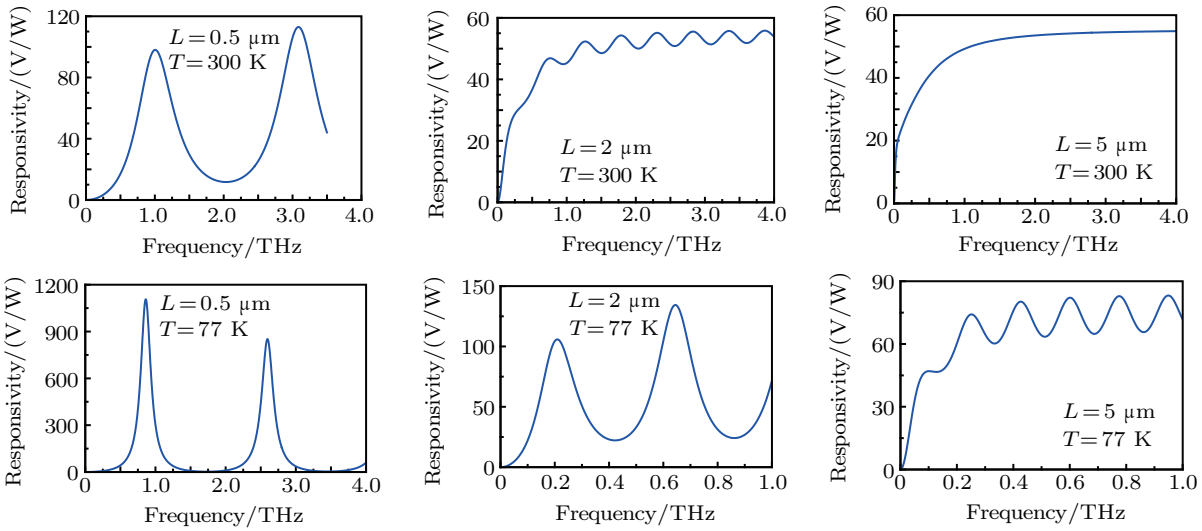


Fig. 6. (color online) Calculation results of theoretical response rate.

By calculation, τ and s can be obtained as shown in Table 4.

Table 4. Relevant simulation results.

Temperature/K	Gate length/μm	$\omega\tau$	$s\tau/L$	$s\sqrt{(\tau/\omega)}/L$
77	0.5	6.01	3.18	1.42
	2	1.27	1.02	0.72
	5	0.51	0.45	0.45
300	0.5	1.55	1.08	0.79
	2	0.39	0.25	0.40
	5	0.15	0.10	0.25

According to the theory proposed by Dyakonov, combining Fig. 6 and Table 4, when $\omega\tau > 1$ and $L < s\tau$, the damping of the plasma oscillations excited by the incoming radiation is small, and the detection signal is dominated by the resonance response. When $\omega\tau < 1$, meanwhile $L > s\tau$ or $L > s\,(\tau/\omega)^{1/2}$, the plasma oscillations are overdamped and the detection signal is mainly of a non-resonant response. So, the resonance detection can be changed by the gate length and the carrier concentration. The resonant response is usually realized at low temperature, and belongs to the narrowband detection;[23] however, the comparison shows that the non-resonant response can be realized at room temperature and has broadband characteristics.

The contrasting results can be seen: the smaller the gate length, the higher the theoretical response rate of terahertz wave is. The theoretical response rate of 300 K can reach 110 V/W at $L = 500$ nm, and the theoretical response at low temperature is higher than 1100 V/W under the same gate length. This result is far higher than that in the case of the GaAs-based HEMT terahertz detector.[24]

When the terahertz frequency is 200 GHz, the theoretical response rates of 2 μm gate length device are 26 V/W (300 K) and 105 V/W (77 K) respectively, with the material optimized in this paper, and the resonant response peak can be generated at 77 K as shown in Fig. 7. The fabrication of 2 μm gate length can be realized by photolithography during the processing, which can effectively reduce the cost and production cycle of the device.

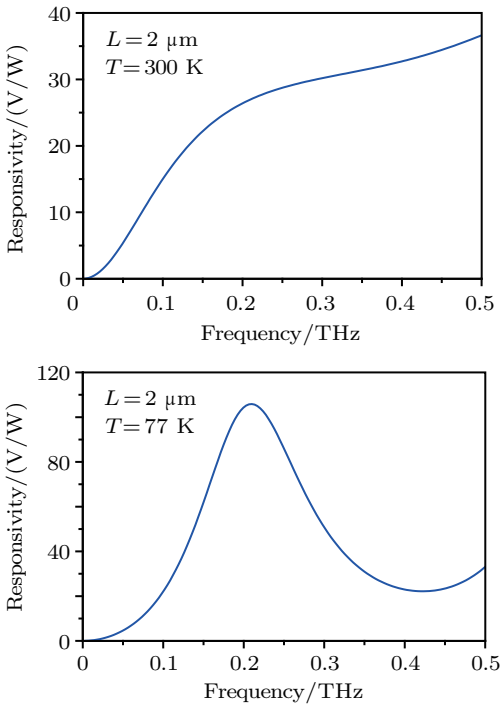


Fig. 7. (color online) Calculation results of theoretical response rate.

5. Conclusions

The InP-based HEMT materials have been prepared by an MBE system. Through using the Hall measurement method and comparing the effects of different In content, InAlAs spacer layer thickness, and two kinds of doping methods, the $In_xGa_{1-x}As/In_{0.52}Al_{0.48}As$ channel 2DEG characteristics are analyzed. The carrier mobilities of 10289 $cm^2/V{\cdot}s$ (300 K)

and 42040 $cm^2/V{\cdot}s$ (77 K) are obtained, and the values of corresponding carrier concentration (N_c) are $3.465\times10^{12}/cm^2$ and $2.502\times10^{12}/cm^2$, respectively. Considering the effect of gate width on terahertz response rate, the theoretical response rate is calculated by the shallow water wave instability theory, and the response rates of terahertz under different gate lengths are compared. When the terahertz frequency is 200 GHz, the theoretical response rates of 2-μm gate length device are 26 V/W (300 K) and 105 V/W (77 K) respectively, with the material optimized in this paper, which lays the foundation for further research and preparation of InP-based HEMT terahertz detectors.

References

[1] Cao J C 2012 *Semiconductor terahertz sources, detectors and applications* (Beijing: Science Press) p. 1 (in Chinese)

[2] Xu J X, Li J L, Wei S H, Ma B, Zhang Y, Zhang Y, Ni H Q and Niu Z C 2017 *Chin. Phys. B* **26** 088702

[3] Qin H, Huang Y D, Sun J D, Zhang Z P, Yu Y, Li X and Sun Y F 2017 *Chin. Opt.* **10** 51

[4] Sizov F, Rogalski A 2010 *Prog. Quantum Electron.* **34** 278

[5] Dyakonov M, Shur M 1993 *Phys. Rev. Lett.* **71** 2465

[6] Victor R, Irina K, Maxim R and Akira S 2007 *International Journal of High Speed Electronics and Systems* **17** 521

[7] Huang J, Guo T Y, Zhang H Y, Xu J B, Fu X J, Yang H and Niu J B 2010 *J. Semicond.* **31** 074008

[8] Taiichi O 2011 *Progress In Electromagnetics Research Symposium Proceedings*, March 20–23, 2011, Marrakesh, Morocco, p. 1266

[9] Taiichi O, Takayuki W, Stephane A B T, Akira S, Victor R, Vyacheslav P and Wojciech K 2014 *Opt. Eng.* **53** 031206

[10] Dyakonov M, Shur M 1996 *IEEE Trans. Electron Dev.* **43** 1640

[11] LU J Q, Shur M S, Hesler J L and Sun L 1998 *IEEE Electron Dev. Lett.* **19** 373

[12] Koo B H, Hanada T, Makino H, Chang J H and Yao T 2001 *J. Crystal Growth* **229** 142

[13] Zhou S X, Qi M, Ai L K and Xu A H 2016 *Chin. Phys. B* **25** 096801

[14] Wang H P, Wang G L, Yu Y, Xu Y Q, Ni H Q, Niu Z C and Gao F Q 2013 *Acta Phys. Sin.* **62** 194205 (in Chinese)

[15] Duque C A, Akimov V, Demediuk R, Belykh V, Tiutiunnyk A, Morales A L, Restrepo R L, Nalivayko O, Fomina O, Mora-Ramos M E and Tulupenko V 2015 *Superlattices and Microstructures* **87** 5

[16] Daoudi M, Dhifallah I, Ouerghi A and Chtourou R 2012 *Superlattices & Microstructures* **51** 497

[17] Wang L M and Cao J C 2008 *J. Semicond.* **29** 1357

[18] Collin R E 1985 *Antennas and Radiowave Propagation* (New York: McCraw Hill) p. 79

[19] Seliuta D, Kašalynas I, Tamošiūnas V, Balakauskas S, Martūnas Z, Ašmontas S, Valušis G, Lisauskas A, Roskos H G and Köhler K 2006 *Electron. Lett.* **42** 825

[20] Guo N, Hu W D, Chen X S, Wang L and Lu W 2013 *Opt. Express* **21** 1606

[21] Liu H R, Yu J S, Peter H and Byron A 2013 *Int. J. Anten. Propag.* **3** 607

[22] Dyer G C, Vinh N Q, Allen S J, Aizin G R, Mikalopas J, Reno J L and Shaner E A 2010 *Appl. Phys. Lett.* **97** 193507

[23] Knap W, Deng Y, Rumyantsev S, Lü J Q, Shur M S, Saylor C A and Brunel L C 2002 *J. Appl. Phys.* **91** 9346

[24] Li J L, Cui S H, Xu J X, Yuan Y, Su X B, Ni H Q and Niu Z C 2017 *J. Infrared Millim. Waves* **36** 790 (in Chinese)